Electronic Supplementary Material (ESI) for ChemComm.
This journal is © The Royal Society of Chemistry 2014

A High Rotational Barrier For Physisorbed Hydrogen in an fcu-Metal–Organic Framework

Tony Pham,[†,§] Katherine A. Forrest,[†,§] Peter A. Georgiev,[‖,○] Wiebke Lohstroh,[⊥] Dong-Xu Xue,[‡] Adam Hogan,[†] Mohamed Eddaoudi,[†,‡] Brian Space,[†] and Juergen Eckert[*,†]

[†]*Department of Chemistry, University of South Florida, 4202 East Fowler Avenue, CHE205, Tampa, FL 33620-5250, United States*

[‖]*Department of Structural Chemistry, University of Milan 21 Via G. Venezian, I-20133 Milan, Italy*

[○]*Faculty of Chemistry and Pharmacy, University of Sofia 1 James Bourchier Blvd., Sofia 1164, Bulgaria*

[⊥]*Heinz Maier-Leibnitz Zentrum (MLZ), Technische Universität München, Lichtenbergstraße 1, D-85748 Garching, Germany*

[‡]*Advanced Membranes and Porous Materials Center Division of Physical Sciences and Engineering 4700 King Abdullah University of Science and Technology (KAUST) Thuwal 23955-6900, Kingdom of Saudi Arabia*

[§]Authors contributed equally

[*]juergen@usf.edu

Crystal Configurations

Parametrization of Y-FTZB is complicated by the random orientations of the $FTZB^{2-}$ linkers ($FTZB^{2-}$ = 2-fluoro-4-(tetrazol-5-yl)benzoate) with respect to the Y^{3+} ions. The ionic clusters, composing of six metal ions, with each being coordinated to four μ_3–OH groups to form a roughly spherical $[Y_6(\mu_3\text{–}OH)_8]^{10+}$ molecular building block (Figure S1(a)), are well defined in the X-ray crystal structure of the MOF, with the exception of the unresolved hydrogen atoms whose positions were determined *via* geometry optimization. However, the 12 $FTZB^{2-}$ linkers (Figure S1(b)) that are coordinated to each cluster show considerable positional variation. The linkers are randomly aligned with respect to the functionality (tetrazolate or carboxylate) coordinated to any given set of Y^{3+} ions, a right/left hand orientation of the fluorine functionality, and two rotational ring positions. This leads to a total of eight distinct occupation sites for a given linker.

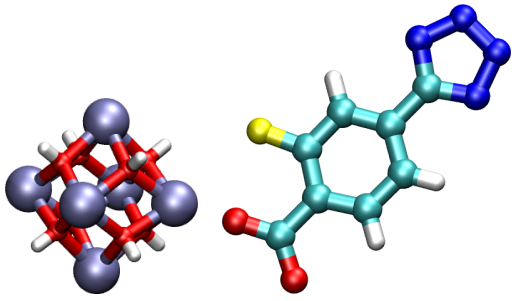

(a) (b)

Figure S1. Molecular building blocks of Y-FTZB: **(a)** $[Y_6(\mu_3\text{–}OH)_8]^{10+}$ cluster and **(b)** $FTZB^{2-}$ linker. Atom colors: C = cyan, H = white, N = blue, O = red, F = yellow, Y = lavender.

For the determination of the atomic positions that are capable of representing the full positionally disordered structure, some sensible approximations were made. In the case of the rotational ring orientations, for which the dihedral angle with regards to the planar carboxylate/tetrazolate alignment is ±4.7°, the variation was considered to be negligible and the selections were random. While the co-location of single bonded functional groups is consistent with local mobility (i.e., components capable of rotation), that is not believed to be the case for this structure. Rather, the deviation from the planarity of the linker is attributed to the optimal low energy accommodation for the fluorine functionality with respect to the neighboring linker functionailties. As such, the two ring orientations are a result of the fluorine disorder and have no capacity to interconvert. This supposition was supported by examining the crystal structure of the MOF, Tb-TZB, referred to as compound 3 in the work of Xue *et al.*[1] This compound is isostructural with Y-FTZB and possesses the same constituents with the exception of the metal and the linkers. This MOF consists of TZB^{2-} linkers, which are the unfluorinated counterparts of the $FTZB^{2-}$ linkers. In this structure, no deviation from linker planarity was observed, though the linker head orientation remains random. It is considered unlikely that the addition of a highly electronegative fluorine atom with a considerably larger atomic radius than hydrogen would result in increased linker mobility.

In the case of the left/right hand fluorine orientation, these positional selections were again made randomly. It is expected

that the adjacent fluorine positions are sufficiently distant (approximately 4.5 Å for the configuration minimizing the interfluorine distance and considerably larger for other alignments) as to make the effect on the electronic structure of these neighboring linkers negligible. Note, the linker alignment with respect to the $[Y_6(\mu_3\text{–}OH)_8]^{10+}$ clusters cannot be dismissed as insignificant. A Y^{3+} ion that is coordinated to a tetrazolate group will have a different electronic structure than an ion that is coordinated to a carboxylate group. As each Y^{3+} ion is coordinated to four linkers, the situation of an ion with only a single functional group attached to it will be the least probable. The number of possible linker orientational conformations about a given metal corresponds to:

$$\omega = C^L \tag{1}$$

where ω is the number of orientational linker combinations, C is the number of conformations for each linker, and L is the number of linkers coordinated to each ion. This yields a total of 16 possibilities for the MOF studied. However, this number does not account for the symmetry leading to degenerate configurations. A total of six nondegenerate linker arrangements with respect to a Y^{3+} ion exist. In the physical crystal structure, an equal *a priori* probability for any given configuration is assumed. Y^{3+} ions that are coordinated to 4 tetrazolate or 4 carboxylate groups (here denoted configurations **1** and **2**, respectively, see Figures S2(a) and S2(b)) are considered non-degenerate states and each have a 1/16 probability of observance. Y^{3+} ions that are coordinated to 3 tetrazolate or 3 carboxylate groups (configurations **3** and **4**, respectively, see Figures S2(c) and S2(d)) as well as those with two adjacent linkers of like orientation (configuration **5**, see Figure S2(e)) each have four–fold degeneracy, resulting in a 4/16 probability of observance apiece. The final configuration with alternating linker orientations (configuration **6**, see Figure S2(f)) is observed in 2/16 of Y^{3+} ions.

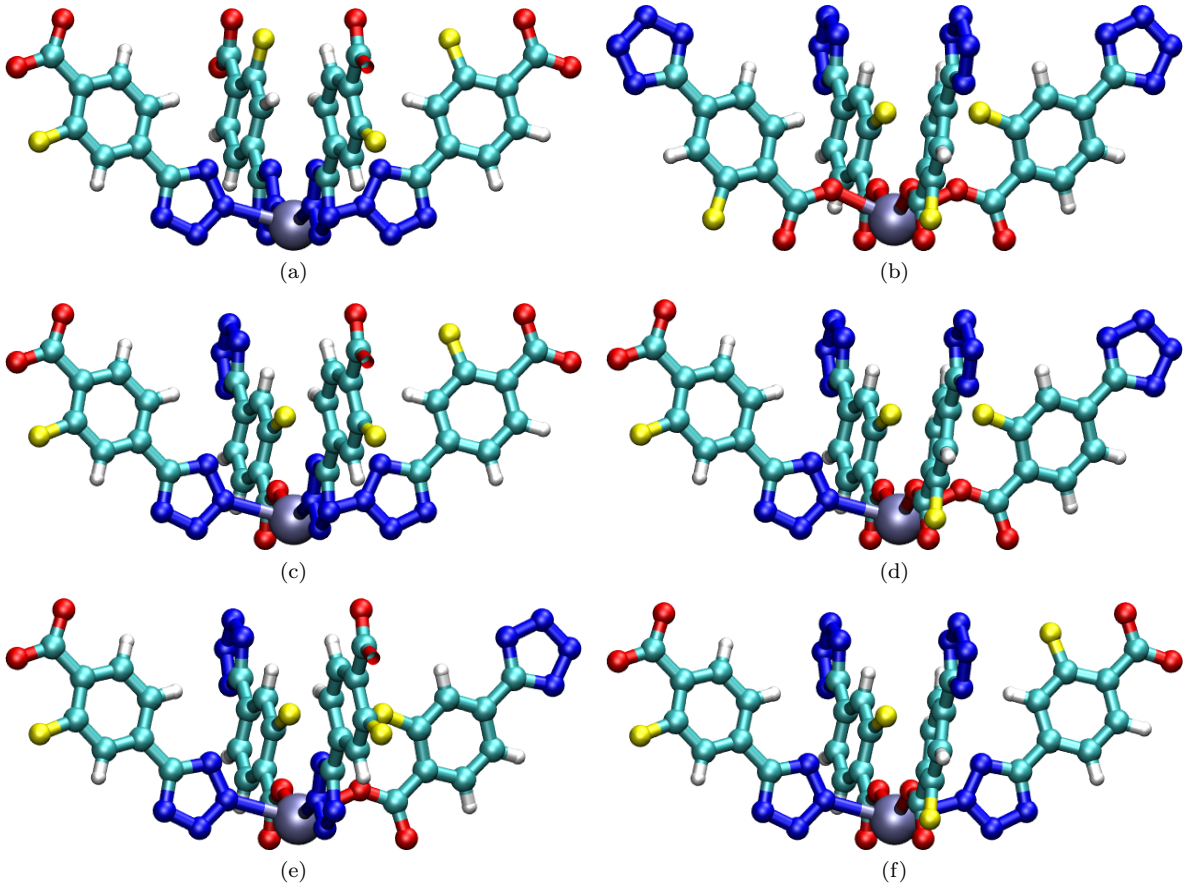

Figure S2. The six possible linker/Y^{3+} ion configurations of Y-FTZB: **(a)** configuration **1**, **(b)** configuration **2**, **(c)** configuration **3**, **(d)** configuration **4**, **(e)** configuration **5**, and **(f)** configuration **6**. Atom colors: C = cyan, H = white, N = blue, O = red, F = yellow, Y = lavender.

A unit cell in which all Y^{3+} ions corresponded to configuration **5** was considered (here denoted structure **1**, see Figure S4(a)). Configuration **5** was chosen from the three most frequently observed orientations in order to preserve the symmetry of the crystal structure. This arrangement resulted in two distinct linker-cluster arrangements. In the first, two tripods of the tetrazolate oriented linkers exist in diametrically opposed positions on the cluster with a ring of the carboxylate oriented linkers forming a ring in between them, while the second has carboxylate tripods and a tetrazolate ring (Figure S3). Of the four clusters extant in a single unit cell, two had the first arrangement and the others had the second.

The positions of the cationic dimethylammonium counterions also had to be determined. Eight of these ions were required in one unit cell to balance the charge of the anionic framework. While these ions are resolved in the X-ray crystal structure,

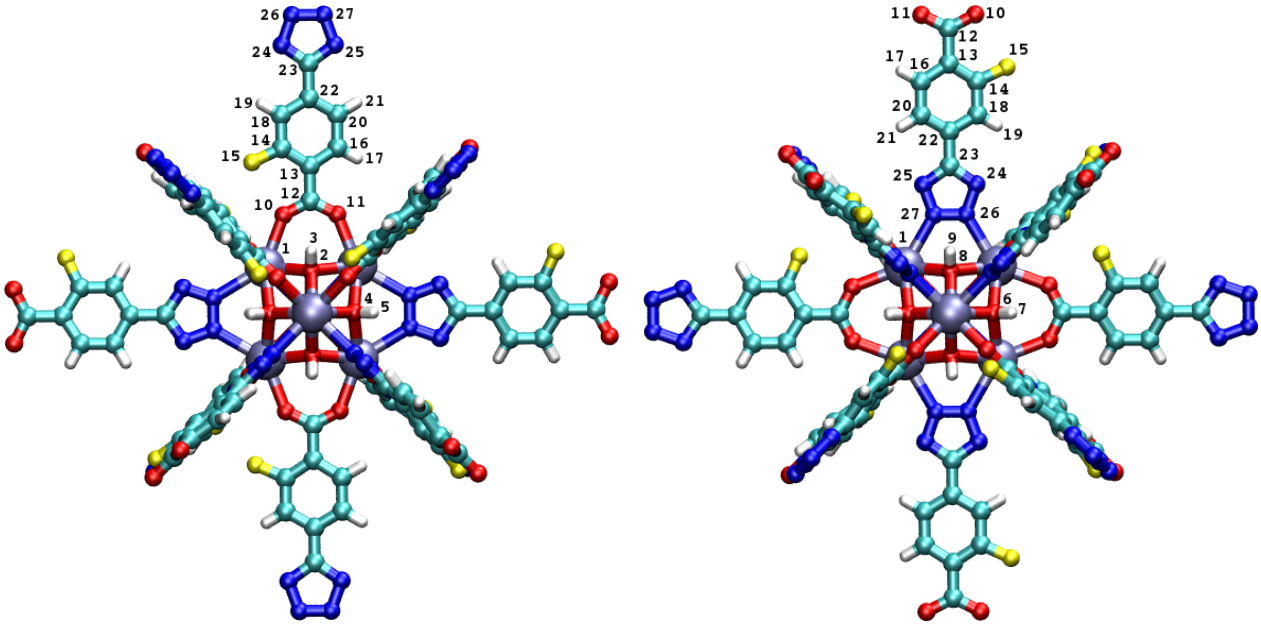

Figure S3. Two cluster-linker alignments observed in structure **1** with all atoms considered chemically distinguishable. Atom colors: C = cyan, H = white, N = blue, O = red, F = yellow, Y = lavender.

the plethora of sites made available by the observed high symmetry in the positionally disordered crystal structure resulted in considerably more localized ions than the eight predicted. Furthermore, considering the fact that no information about the preferred environment of the counterions with respect to the disordered functionality could be obtained from the structure and the fact that the X-ray crystal structure was taken prior to activation (thus, raising the possibility of solvent interaction effecting the sorption site about the counterions), it was decided that the $(CH_3)_2NH_2^+$ counterions would be separately parametrized and the positions were determined *via* simulated annealing in the canonical ensemble as described below (see Canonical Monte Carlo section).

While the simulated hydrogen uptake at 77 K and 87 K in this structure is consistent with experiment, the initial isosteric heat of adsorption (Q_{st}) value is notably lower. This result is consistent with the existence of a small number of superior sorption sites in the physical crystal that is not represented in the modeled structure. As a result, a second unit cell (here denoted structure **2**, see Figure S4(b)) was parametrized. In this variant, the same approximations regarding the ring and fluorine orientations were made while the linker configurations about the 24 Y^{3+} ions were chosen to reflect orientations **1**, **2**, **3**, **4**, and **6** in the proper probabilistic proportions. Together, the two structures exhibit all possible metal/linker conformations. Structure **2** produced a similar uptake to structure **1**, but with a significantly higher initial H_2 Q_{st} value that is close to the experimental value for Y-FTZB. The primary sorption site to which this value corresponds to consists of a Y^{3+} ion that is coordinated to four tetrazolate functional groups (an alignment only extant in structure **2**) and in proximity to a dimethylammonium counterion.

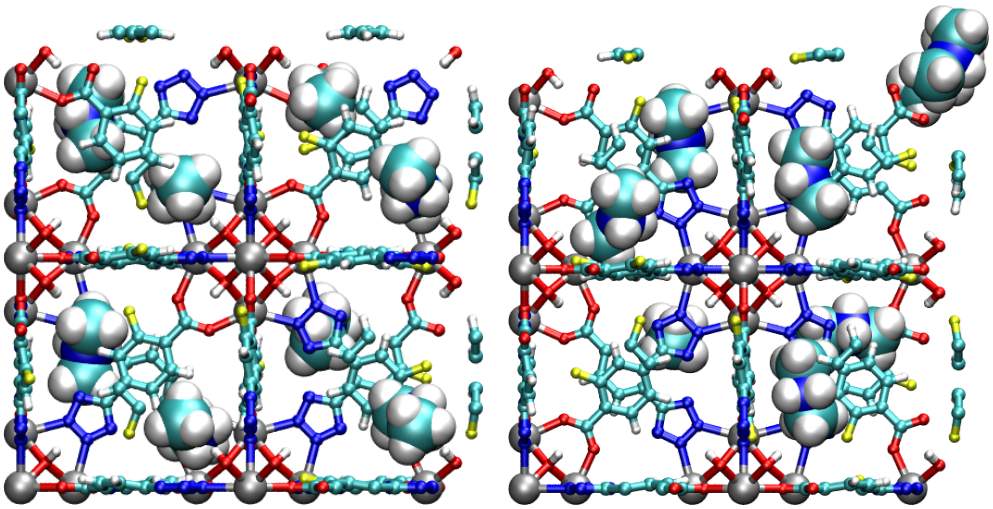

(a) (b)

Figure S4. The $a/b/c$ axis view of the unit cell of **(a)** structure **1** and **(b)** structure **2** of Y-FTZB. Structure **2** was used for the simulations in this work. The $(CH_3)_2NH_2^+$ counterions are shown in van der Waals representation. Atom colors: C = cyan, H = white, N = blue, O = red, F = yellow, Y = silver.

Parametrization

The potential energy of Y-FTZB is a function of repulsion/dispersion parameters, atomic point partial charges, and atomic point polarizabilities that are localized on the nuclear center of all atoms of the MOF. The Lennard-Jones 12–6 potential[2] was used to model repulsion/dispersion interactions, and these parameters for all MOF atoms were taken from the Universal Force Field (UFF).[3] The partial charges for the atoms in Y-FTZB were determined from electronic structure calculations on several fragments that were taken from the crystal structure of the MOF. More details of these calculations can be found in the next section. The polarizabilities for all C, H, N, O, and F atoms were taken from a carefully parametrized and transferable set based on the work by van Duijnen and Swart.[4] The polarizability parameter for Y^{3+} was calculated for the isolated cation using the DFT functional PBE0, the def2-QZVPP basis set with effective core potentials and using the SCF program ORCA[5] to solve the coupled-perturbed SCF equations. A value of 0.60159 $Å^3$ was calculated as the polarizability for Y^{3+}.

Electronic Structure Calculations

The electrostatic environment of Y-FTZB was approximated using partial charges localized on the atomic positions. These charges were determined by perfoming electronic structure calculations on a series of representational fragments that were taken from the crystal structure of the MOF. Chemical termination was achieved by the addition of hydrogen atoms where appropriate. Hartree–Fock methods were used to calculate the electrostatic potential surface of each fragment and the partial charges were fitted to reproduce the potential at a large number of points along the surface using the CHELPG method.[6,7] The NWChem simulation package[8] was used with the 6-31G* basis set applied for all first and second row elements. This basis set has been shown to produce overpolarized charges for gas phase fragments that are consistent with condensed phase media.[9] For the Y^{3+} ions, the LANL2DZ[10–12] effective core potential basis set was employed for sensible treatment of the inner core electrons of this many-electron species. Discarding terminal atoms whose environments do not approximate MOF conditions, the charges were evaluated for each chemically distinct atom in the fragment. These charges were then averaged over all fragments to obtain the charges that were used in the simulation.

Note, prior to charge fitting, the determination of the chemically distinguishable atoms was required. The positionally disordered structure of Y-FTZB is highly symmetric, with each Y^{3+} ion, μ_3–OH group, and $FTZB^{2-}$ linker being in a chemically indistinguishable location from every other component of its type. This yielded a total of 21 chemically distinct atoms. The selection of linker orientaions as described above breaks down the structural symmetry, leading to a prohibitively large number of positionally distinguishable atoms. As a consequence, the structure was examined to determine psuedo-degenerate atoms, i.e., those in sufficiently similar environments as to make them identical to within simulation precision.

Structure **1**, described in the Crystal Configurations section, was considered first. For this higher symmetry crystal structure, the Y^{3+} ions are considered interchangeable as the orientation of the central ring of the linker and its attendant fluorine atom are considered sufficiently distant as to have a negligible electrostatic effect on the metal ions. In both clusters, each ion is coordinated to two tetrazolate and two carboxylate groups, thus giving them similar environments. Charge fitting of similar fragments of both cluster types yielded similar charges (Table S1), indicating that this assumption is viable. Because there is one linker of similar alignment and two of dissimilar alignment with respect to their Y^{3+}-coordinated functional group, this sensible approximation was made to treat them as interchangable. Additional asymmetric effects from variant central ring and/or fluorine orientations are again considered sufficiently distant to be disregarded.

Initially, the μ_3–OH groups were consided to be chemically interchangable. However, examination of the fragment charges revealed significant alterations in the charge magnitudes depending on the identity of the Y^{3+}-coordinated functional groups surrounding the hydroxide ion. The charge separation on the hydroxyl oxygen atom for the two extreme situations of three carboxylate–metal oriented linkers compared to three tetrazolate–metal oriented linkers is more negative than $-1.0\ e^-$ despite the homogeneity of the coordinated metal ions charges (Table S1). As such, the hydroxide ions were divided into four chemically distinct sets: those surrounded by carboxylate groups, those surrounded by tetrazolate groups, and the two sets with one coordinated carboxylate/tetrazolate and two of the other moiety. Thus, the number of chemically distinct atoms increased from 21 to 27. Sixteen fragments were selected to give a well averaged value for each chemically distinct atom (Figure S5). The final calculated partial charges for the chemically distinct atoms in structure **1** of Y-FTZB are provided in Table S3.

Parametrization of structure **2**, which was undertaken after the failure of structure **1** to accurately model the physical crystal (as discussed in the Crystal Configurations section), was a slightly more complex problem. Five distinct Y^{3+} ions exist in structure **2** with respect to the linker coordination environments, none of which correspond to the ion observed in structure **1**. As expected, examination of fragments containing these ions yielded a wide range of partial charges, with the maximal charge having more than twice the minimal value and with an absolute magnitude greater than $1.0\ e^-$. Note, the fragments that were selected for structure **2** are shown in Figure S7, and the calculated partial charges for the chemically distinct atoms on each fragment can be found in Table S2. The μ_3–OH groups in this structure, which are caught between chemically distinct Y^{3+} ions as well as variant linker functionality, produced a new set of dissimilar charges. A total of six different linker/Y^{3+} environments were identified, with a difference of $0.7\ e^-$ observed between the high and low hydroxyl oxygen charges.

While less homogenously arranged than their counterparts in structure **1** (since the linkers have non-identical Y^{3+} coordination and attendant nearby functionality in structure **2**), the partial charges for the atoms on the linkers in structure **2** are consistent with their counterparts in structure **1** to within joint uncertainties. As such, all linkers in both structures are considered interchangable and, in the interest of maintaining consistency, the partial charges that were determined for the fragments of structure **1** applied to those corresponding to structure **2**. A total of 17 chemically distinct atoms (Figure S6) (five Y^{3+} ions and six μ_3–OH groups) were added to the total number of chemically distinct atoms to give a total of 44. Structures **1** and **2** contain 27 and 35 of these atoms, respectively. The partial charges for the 17 chemically distinguishable atoms observed in structure **2** of Y-FTZB can be found in Table S4. Note, as explained in the Crystal Configurations section, the dimethylammonium counterion was parametrized separately from the framework. The partial charges for the chemically distinct atoms on the $(CH_3)_2NH_2^+$ counterions (Figure S8) are provided in Table S5. These charges were used for the counterions in the simulations in both structures.

Table S1. Comparison of partial charges (e^-) for the series of fragments taken from structure **1** of Y-FTZB. Numbering of atoms corresponds to Figure S3.

Atom	Label	Frag 1	Frag 2	Frag 3	Frag 4	Frag 5	Frag 6	Frag 7	Frag 8	Frag 9	Frag 10	Frag 11	Frag 12	Frag 13	Frag 14	Frag 15	Frag 16
Y	1	1.5184	1.5805	-	1.4969	1.4795	1.6367	1.5086	1.6279	1.5803	1.5529	-	-	-	-	-	-
O	2	-	-	-	-	-	-	-0.2614	-	-0.2465	-0.3075	-	-	-	-	-	-
H	3	-	-	-	-	-	-	0.0950	-	0.0892	0.1130	-	-	-	-	-	-
O	4	-	-	-	-	-	-0.9366	-0.8658	-0.8954	-0.9569	-0.8770	-	-	-	-	-	-
H	5	-	-	-	-	-	0.2212	0.1853	0.2267	0.2275	0.1967	-	-	-	-	-	-
O	6	-0.5317	-0.6292	-	-0.6377	-	-	-	-	-	-	-	-	-	-	-	-
H	7	0.1264	0.1717	-	0.1891	-	-	-	-	-	-	-	-	-	-	-	-
O	8	-1.3674	-1.3174	-1.4084	-1.3205	-	-	-	-	-	-	-	-	-	-	-	-
H	9	0.2834	0.2836	0.3355	0.2703	-	-	-	-	-	-	-	-	-	-	-	-
O	10	-0.7145	-0.6966	-	-0.7082	-0.7118	-0.7100	-0.7163	-0.7126	-0.7298	-0.7175	-0.6547	-0.7124	-	-	-	-
O	11	-0.7664	-0.7670	-	-0.7618	-0.7543	-0.7977	-0.7605	-0.7773	-0.7733	-0.7775	-0.7356	-0.7377	-	-	-	-
C	12	0.9887	0.9595	-	0.9707	0.9894	0.9924	1.0093	0.9504	1.0140	1.0124	0.8777	0.9044	-	-	-	-
C	13	-	-	-	-	-	-	-	-	-	-	-0.2200	-	-0.1354	-	-0.1637	-0.1698
C	14	-	-	-	-	-	-	-	-	-	-	0.3557	-	0.3642	-	0.3920	0.3422
F	15	-	-	-	-	-	-	-	-	-	-	-0.2525	-	-0.2705	-	-0.2764	-0.2300
C	16	-	-	-	-	-	-	-	-	-	-	-0.0696	-	-0.1749	-	-0.1518	-0.0909
H	17	-	-	-	-	-	-	-	-	-	-	0.1501	-	0.1605	-	0.1677	0.1659
C	18	-	-	-	-	-	-	-	-	-	-	-0.1187	-	-0.2539	-	-0.1239	-0.1389
H	19	-	-	-	-	-	-	-	-	-	-	0.1411	-	0.1637	-	0.1234	0.1478
C	20	-	-	-	-	-	-	-	-	-	-	-0.0876	-	-0.0988	-	-0.0182	-0.0948
H	21	-	-	-	-	-	-	-	-	-	-	0.0943	-	0.1109	-	0.0914	0.0980
C	22	-	-	-	-	-	-	-	-	-	-	-0.3060	-	-0.2678	-	-0.3605	-0.2386
C	23	-	0.8904	0.9135	0.8680	-	0.8831	-	0.8756	0.8709	0.8888	-	-	0.9596	0.9085	-	-
N	24	-	-0.6820	-0.6805	-0.6453	-	-0.6921	-	-0.6656	-0.6854	-0.6918	-	-	-0.6578	-0.6484	-	-
N	25	-	-0.6989	-0.6735	-0.6824	-	-0.6822	-	-0.6760	-0.6706	-0.6844	-	-	-0.6724	-0.6734	-	-
N	26	-	0.0943	0.0760	0.0621	-	0.0943	-	0.0515	0.0758	0.0823	-	-	-0.0152	-0.0009	-	-
N	27	-	0.1111	0.0660	0.1185	-	0.0806	-	0.0897	0.0872	0.0847	-	-	0.0232	0.0846	-	-

Table S2. Comparison of partial charges (e^-) for the series of fragments taken from structure **2** of Y-FTZB. Numbering of atoms corresponds to Figure S6.

Atom	Label	Frag 1	Frag 2	Frag 3	Frag 4	Frag 5	Frag 6	Frag 7	Frag 8	Frag 9	Frag 10	Frag 11	Frag 12	Frag 13	Frag 14	Frag 15	Frag 16
Y	1	-	-	-	1.2666	-	-	-	-	1.0417	1.0326	1.0188	1.2323	1.1277	1.0414	1.0177	1.0328
Y	2	1.2284	1.2623	-	-	-	-	-	-	-	1.3000	1.2863	-	-	1.3590	1.3189	1.3330
Y	3	1.7469	1.7269	-	2.0552	1.7373	-	-	-	-	-	-	-	-	-	-	-
Y	4	-	2.0291	-	-	-	1.8334	-	-	-	-	-	-	-	-	-	-
Y	5	-	-	2.3632	-	-	2.3888	2.3638	2.3931	-	-	-	-	-	-	-	-
O	6	-	-	-	-	-	-	-	-	-	-	-0.8201	-	-	-	-0.8096	-0.7417
H	7	-	-	-	-	-	-	-	-	-	-	0.0791	-	-	-	0.0794	0.0595
O	8	-	-	-	-	-	-	-	-	-	-0.3420	-0.3516	-	-	-0.4294	-0.3714	-0.4609
H	9	-	-	-	-	-	-	-	-	-	-0.0137	-0.0065	-	-	-0.0021	0.0047	0.0217
O	10	-1.0142	-0.9926	-	-0.9877	-1.0563	-	-	-	-	-	-	-	-	-	-	-
H	11	0.2095	0.2043	-	0.1976	0.2281	-	-	-	-	-	-	-	-	-	-	-
O	12	-0.5615	-0.5539	-	-0.5965	-	-	-	-	-	-	-	-	-	-	-	-
H	13	0.1174	0.1271	-	0.1347	-	-	-	-	-	-	-	-	-	-	-	-
O	14	-	-	-1.1010	-	-	-1.0217	-1.1153	-1.0385	-	-	-	-	-	-	-	-
H	15	-	-	0.2849	-	-	0.2576	0.3117	0.2632	-	-	-	-	-	-	-	-
O	16	-	-	-	-	-	-0.7433	-0.7278	-0.7823	-	-	-	-	-	-	-	-
H	17	-	-	-	-	-	0.2424	0.2432	0.2785	-	-	-	-	-	-	-	-

Figure S5. Fragments of structure **1** of Y-FTZB that were selected for charge fitting calculations. Atom colors: C = cyan, H = white, N = blue, O = red, F = yellow, Y = lavender.

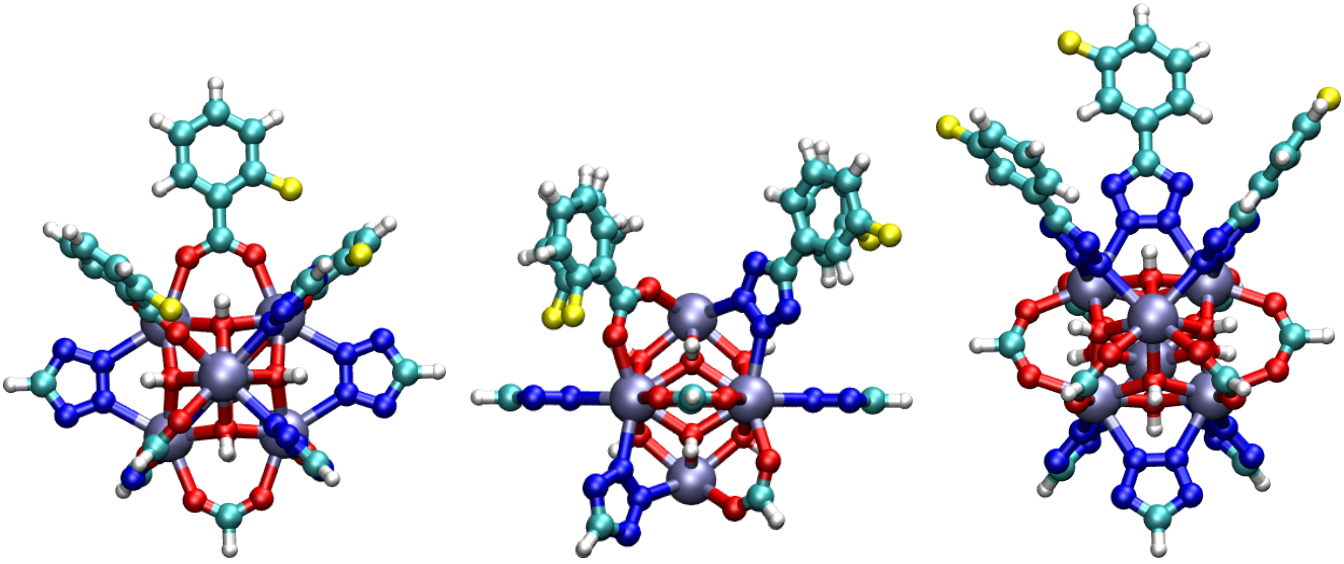

(a)Fragment 1 (b)Fragment 2 (c)Fragment 3

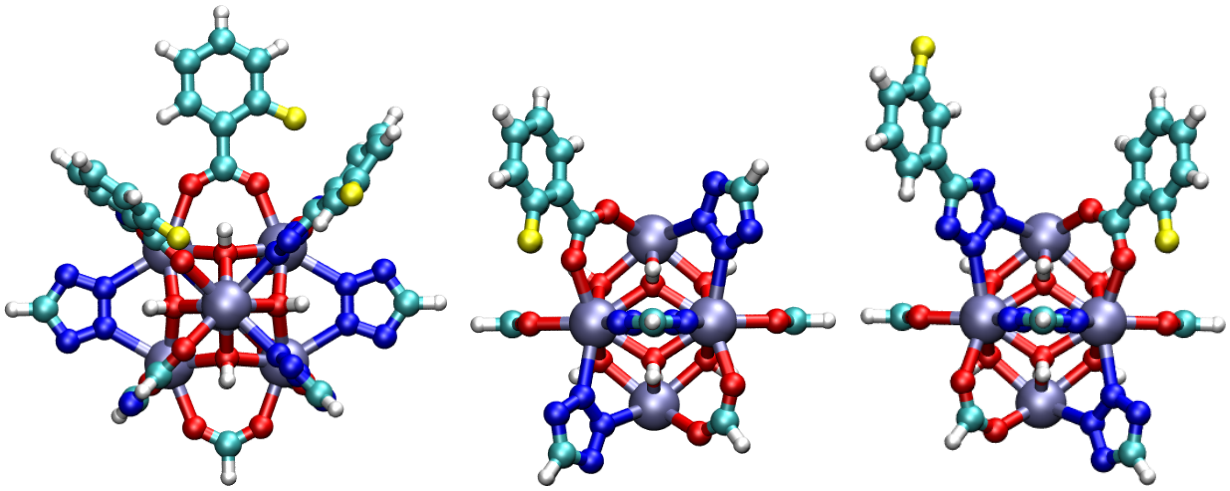

(d)Fragment 4 (e)Fragment 5 (f)Fragment 6

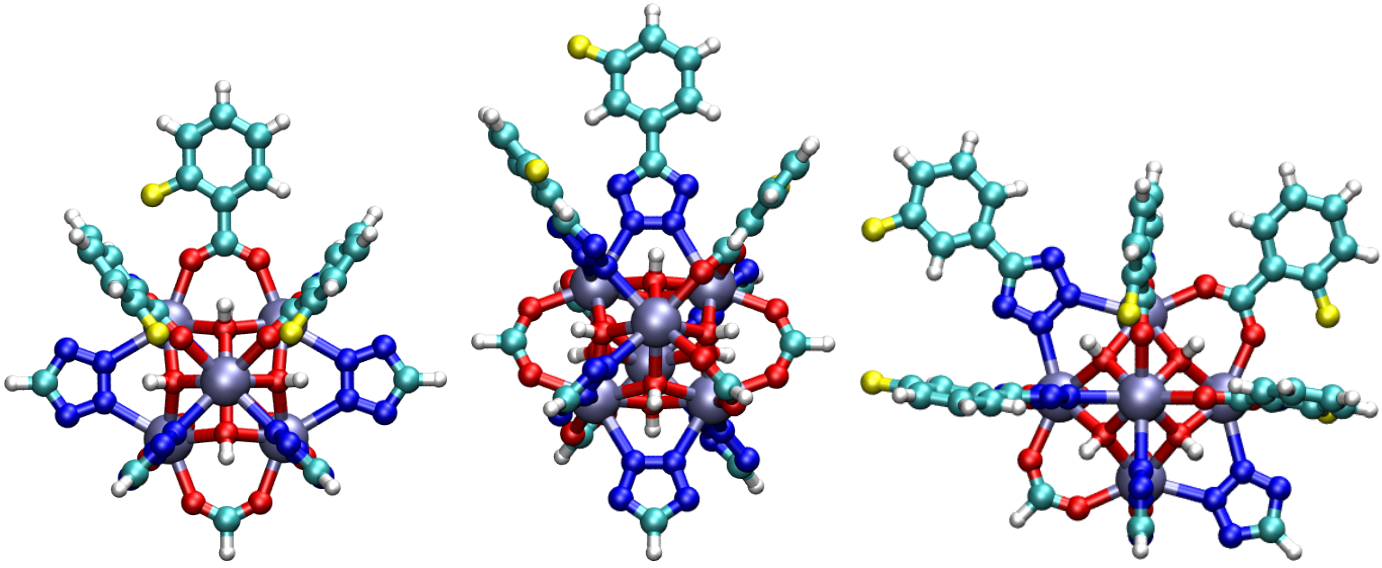

(g)Fragment 7 (h)Fragment 8 (i)Fragment 9

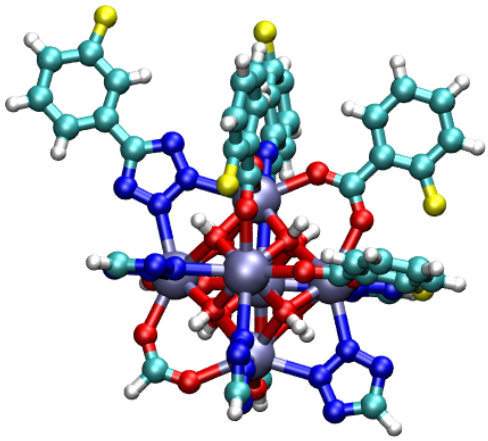

(j)Fragment 10

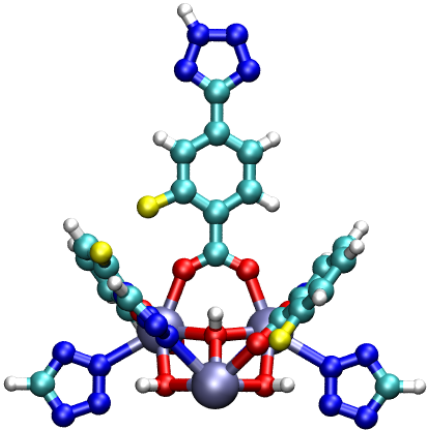

(k)Fragment 11

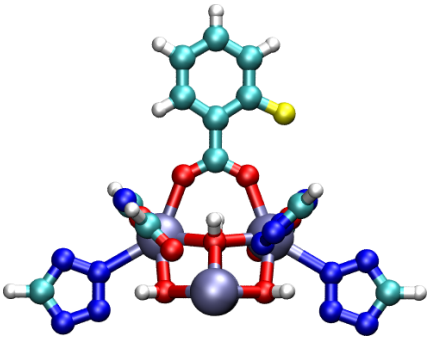

(l)Fragment 12

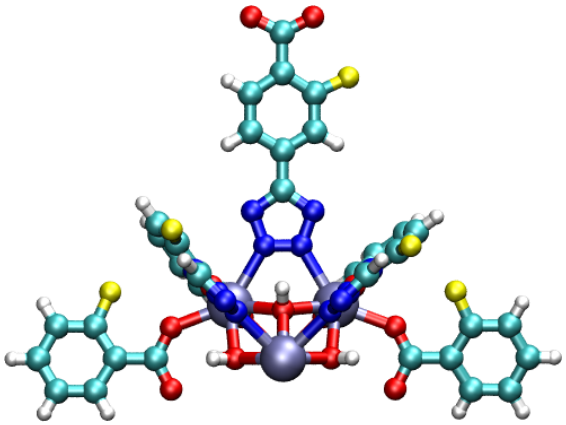

(m)Fragment 13

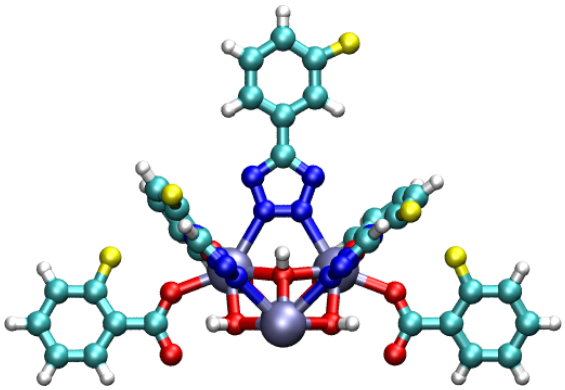

(n)Fragment 14

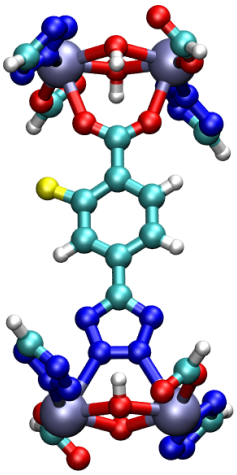

(o)Fragment 15

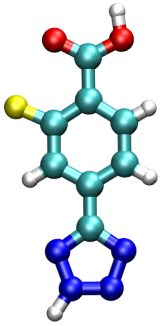

(p)Fragment 16

Figure S6. Four $[Y_6(\mu_3\text{–}OH)_8(FTZB)_{12}]^{14-}$ clusters observed in structure **2** of Y-FTZB. Numerical labeling correspond to chemically distinct atoms not observed in structure **1**. Atom colors: C = cyan, H = white, N= blue, O = red, F = yellow, Y = lavender.

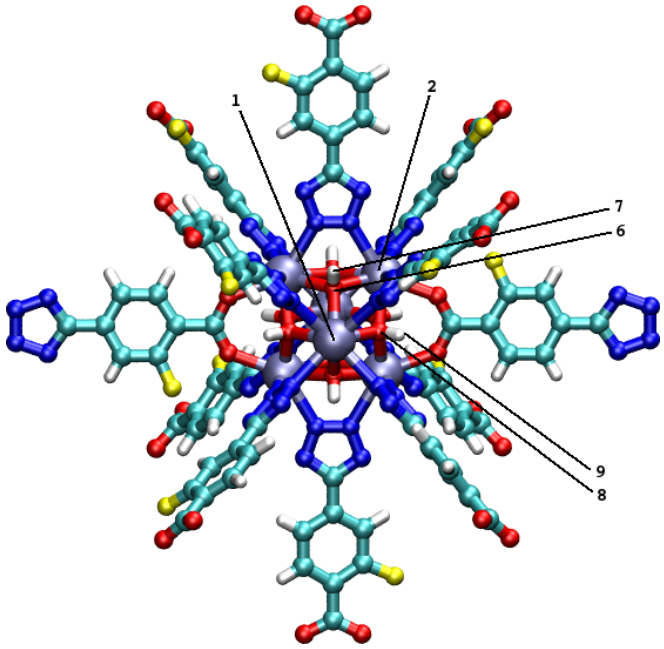

(a)Cluster 1

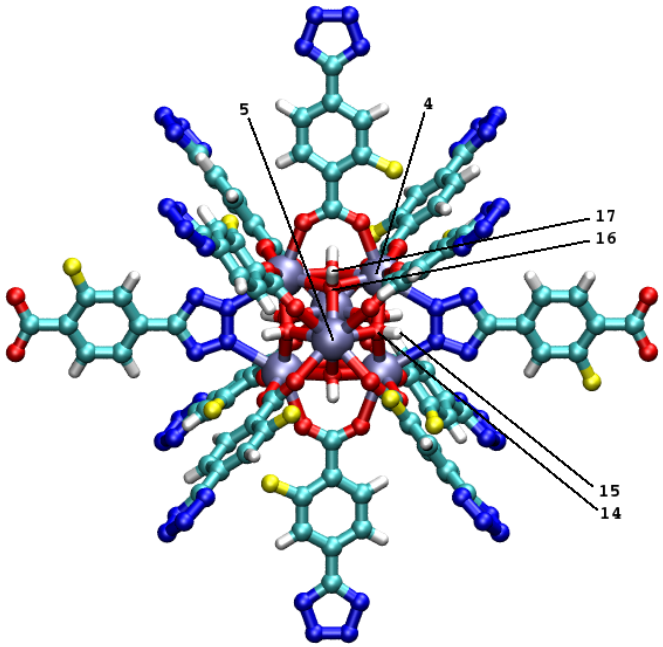

(b)Cluster 2

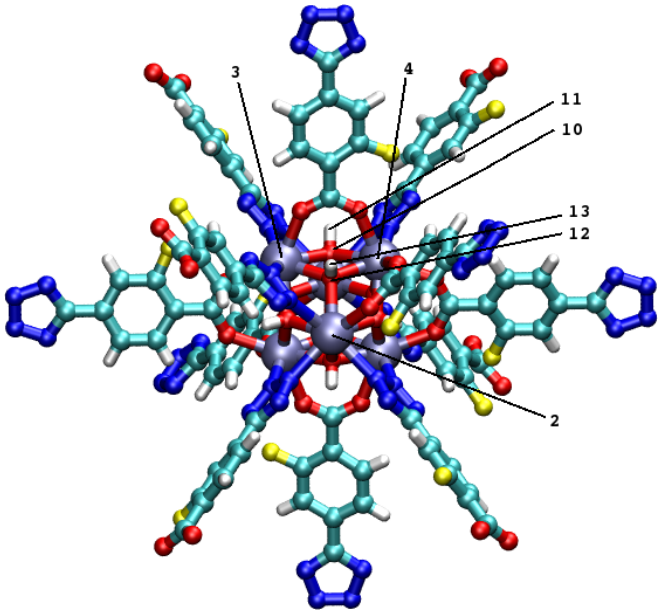

(c)Cluster 3

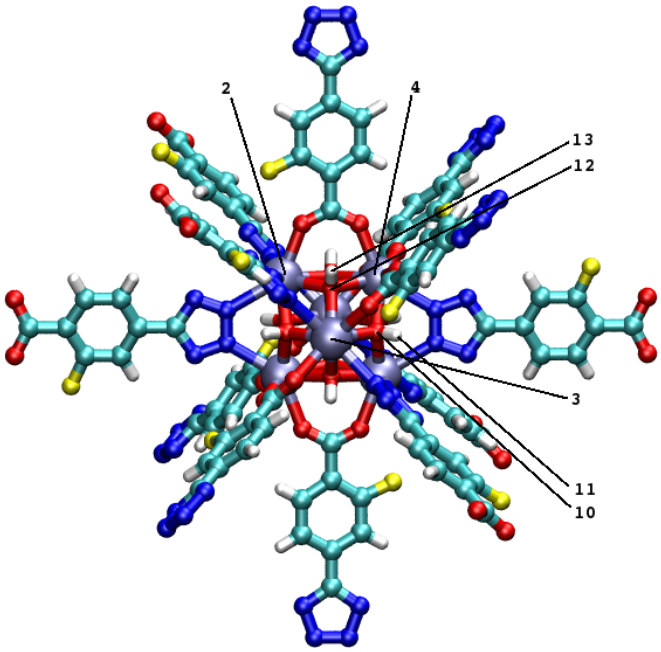

(d)Cluster 4

Figure S7. Fragments of structure **2** of Y-FTZB that were selected for gas phase charge fitting calculations. Numerical labeling correspond to chemically distinct atoms evaluated. Atom colors: C = cyan, H = white, N = blue, O = red, F = yellow, Y = lavender.

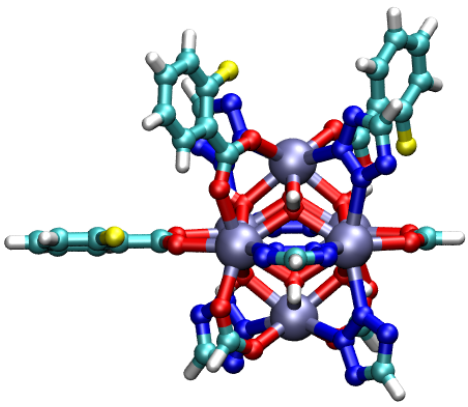

(a)Fragment 1

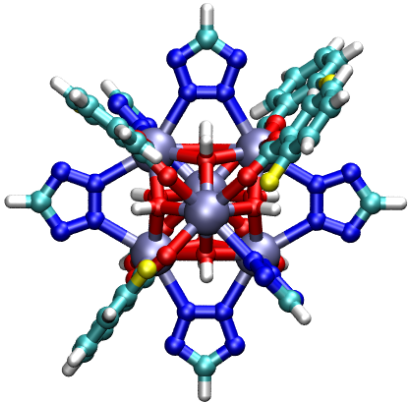

(b)Fragment 2

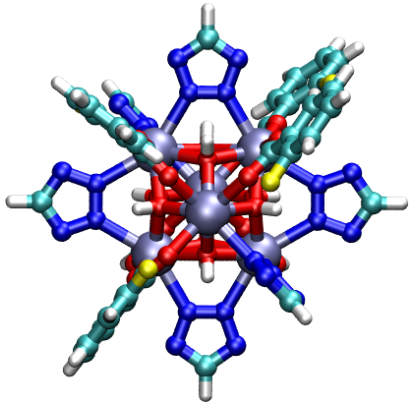

(c)Fragment 3

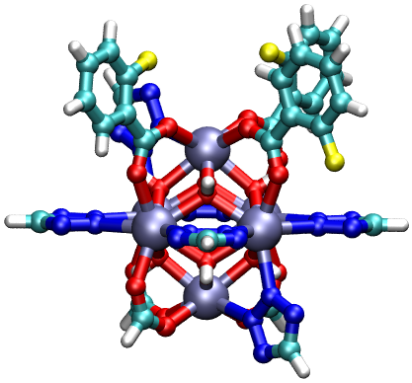

(d)Fragment 4

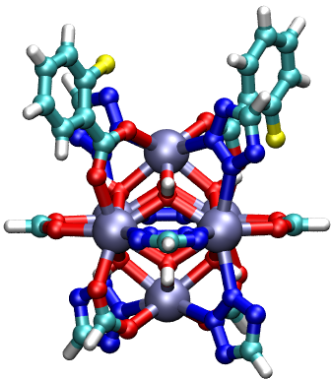

(e)Fragment 5

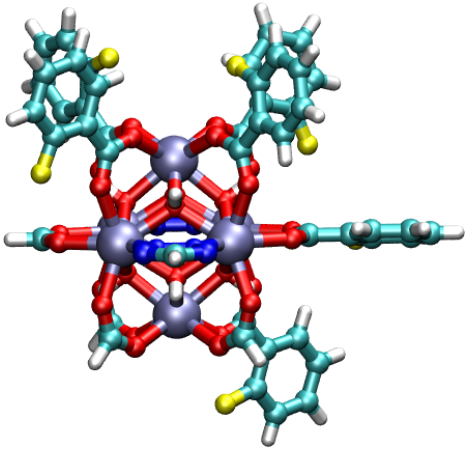

(f)Fragment 6

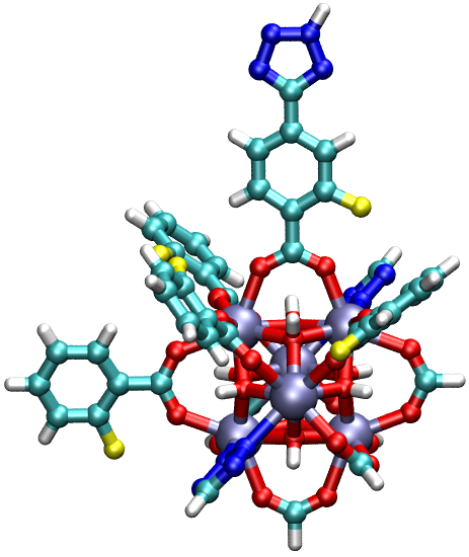

(g)Fragment 7

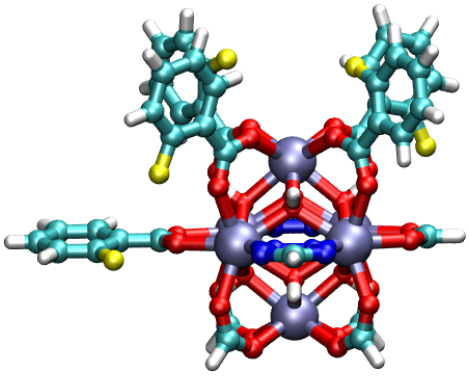

(h)Fragment 8

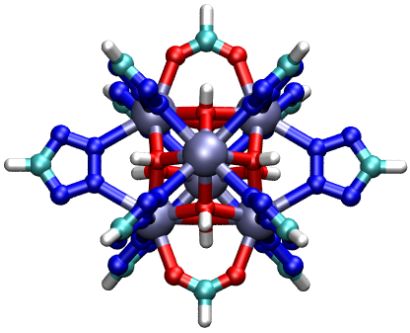

(i)Fragment 9

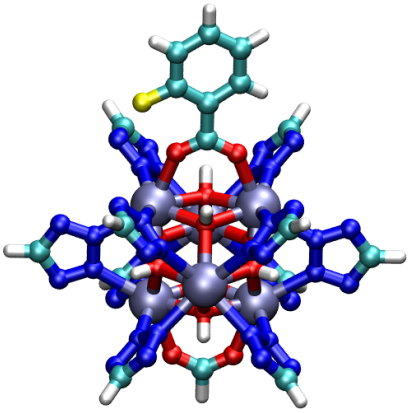

(j)Fragment 10

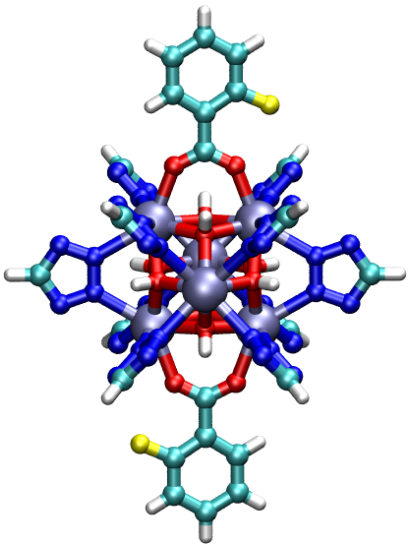

(k)Fragment 11

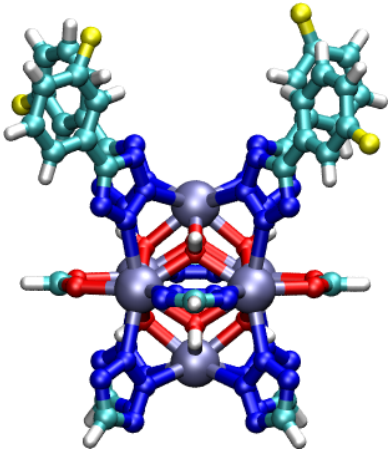

(l)Fragment 12

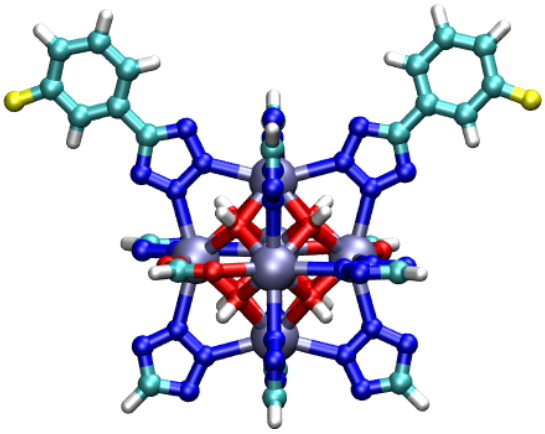

(m)Fragment 13

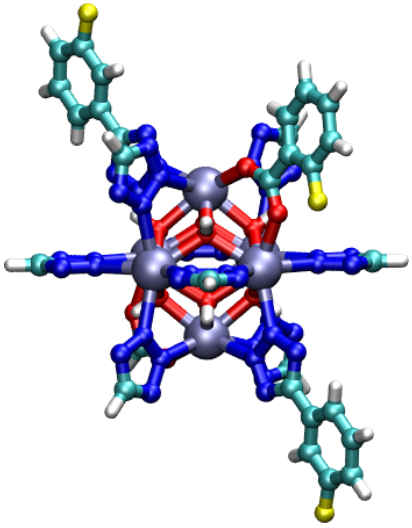

(n)Fragment 14

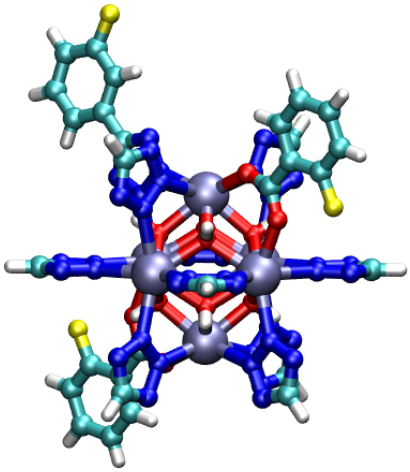

(o)Fragment 15

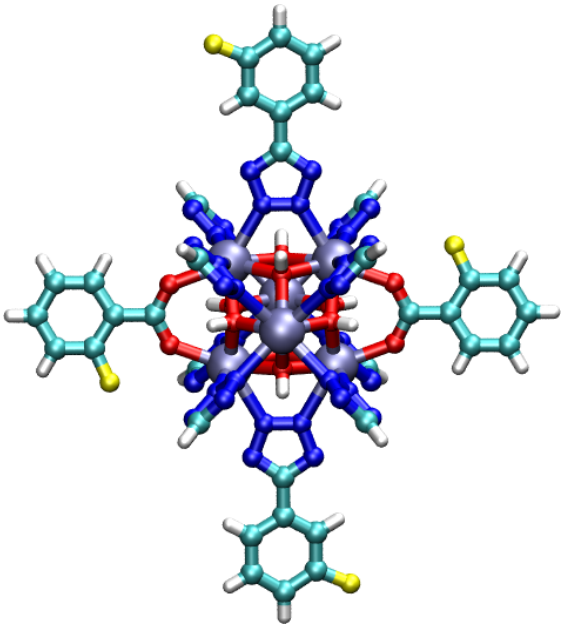

(p)Fragment 16

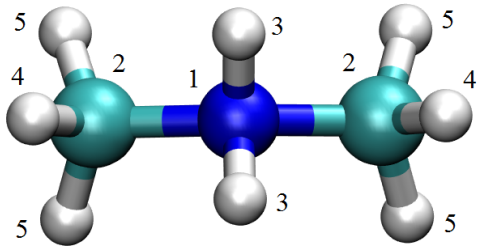

Figure S8. The numbering of the chemically distinct atoms on the $(CH_3)_2NH_2^+$ counterion as referred to in Table S5. Atom colors: C = cyan, H = white, N = blue.

Table S3. Partial charges (e^-) for the chemically distinct atoms in structrure **1** of Y-FTZB. Numbering of atoms corresponds to Figure S3.

Atom	Label	q (e^-)
Y	1	1.55352
O	2	-0.27106
H	3	0.09906
O	4	-0.90386
H	5	0.21148
O	6	-0.59791
H	7	0.16238
O	8	-1.34975
H	9	0.29320
O	10	-0.70575
O	11	-0.76238
C	12	0.96988
C	13	-0.17176
C	14	0.36353
F	15	-0.25665
C	16	-0.12147
H	17	0.16105
C	18	-0.15842
H	19	0.14400
C	20	-0.07465
H	21	0.09865
C	22	-0.29243
C	23	0.89536
N	24	-0.67027
N	25	-0.67746
N	26	0.05780
N	27	0.08283

Table S4. Partial charges (e^-) for the chemically distinct atoms that exist only in structure **2** of Y-FTZB. The partial charges for the atoms on the linkers are consistent with those reported in Table S3 for structure **1**. Numbering of atoms corresponds to Figure S6.

Atom	Label	q (e^-)
Y	1	1.03055
Y	2	1.24881
Y	3	1.67598
Y	4	1.90324
Y	5	2.29367
O	6	-0.79045
H	7	0.07007
O	8	-0.39103
H	9	0.00082
O	10	-1.01268
H	11	0.20248
O	12	-0.57063
H	13	0.12194
O	14	-1.06909
H	15	0.26951
O	16	-0.75113
H	17	0.24573

Table S5. Partial charges (e^-) for the chemically distinct atoms on the the $(CH_3)_2NH_2^+$ counterion. Numbering of atoms corresponds to Figure S8.

Atom	Label	q (e^-)
N	1	0.20260
C	2	-0.19430
H	3	0.22290
H	4	0.12150
H	5	0.12430

H_2 Potential

Table S6. Parameters used to characterize the five–site polarizable H_2 potential[13] used in this work. COM corresponds to the center-of-mass site, H corresponds to the atomic locations of the hydrogen atoms, and OS corresponds to the Lennard-Jones off-site.

Site	r(Å)	ϵ(K)	σ(Å)	q (e^-)	α°(Å^3)
COM	0.00000	12.76532	3.15528	-0.74640	0.69380
H	0.37100	0.00000	0.00000	0.37320	0.00044
H	-0.37100	0.00000	0.00000	0.37320	0.00044
OS	0.36300	2.16726	2.37031	0.00000	0.00000
OS	-0.36300	2.16726	2.37031	0.00000	0.00000

Canonical Monte Carlo

While the eight $(CH_3)_2NH_2^+$ counterions required to neutralize the anionic unit cell were sufficiently immobile to resolve in the crystal structure, these positions were highly disordered as the corresponding CIF file for Y-FTZB (taken from reference 1) reported an occupancy of 0.13 for any of the possible localities. Additionally, the structure was examined prior to activation, as the interactions between the counterions and the solvent molecules could have an effect on the location of the counterions. As a result, for the determination of the counterion positions, these ions were separately parametrized with Lennard-Jones parameters taken from UFF,[3] point polarizabilities taken from van Duijnen and Swart,[4] and partial charge taken from a single ion charge fit using the same methods for the MOF fragments as described earlier (see Electronic Structure Calculations section).

Canonical Monte Carlo simulations (CMC) were performed in both structures **1** and **2** of Y-FTZB (see Crystal Configurations section), with each containing eight mobile dimethyammonium counterions. This method constrains the particle number (N), volume (V), and temperature (T) of the simulation cell to be constant. These simulations were executed with the Massively Parallel Monte Carlo (MPMC) code.[14] The equilibrium positions of the counterions in both structures were determined using simulated annealing. An initial temperature of 500 K was used in order to encourage the ions to explore the systems prior to settling into the minima. Due to the highly variable sorption environement in this MOF, especially for structure **2**, the annealed positions were then used as initial positions for new simulated annealing runs in an attempt to avoid settling into the local minima. This was continued for several iterations with lower energy positions retained and higher energy positions disregarded to obtain the lowest possible energy. Once these sites were determined, the positions of the dimethylammonium counterions were held rigid for the simulations of H_2 sorption in Y-FTZB as described in the Grand Canonical Monte Carlo section below.

In both structures, the eight dimethylammonium counterions were initially located in the centers of the tetrahedral cages of the MOF. Simulated annealing calculations in structure **1** revealed that these counterions settled into the corners formed by a tripod of tetrazolate groups (existing in four cages) and two tetrazolate/one carboxylate corners otherwise (Figure S4(a)). Structure **2** had a predictably less well-ordered result, with four counterions localized in the tetrazolate tripods, two counterions localized in the 2 tetrazolate/1 carboxylate tripods (again, in cages without the former functionality), and two counterions localized in proximity to the open-metal sites (Figure S4(b)). Specifically, the latter two counterions positioned near the Y^{3+} ions that are coordinated to three tetrazolate and one carboxylate moieties, which are labeled atom 2 in Figure S6. Notably, a number of metal sites with this linker coordination remain open for sorbate interactions.

Grand Canonical Monte Carlo

Simulations of H_2 sorption in Y-FTZB were performed using grand canonical Monte Carlo (GCMC) in a single unit cell of the MOF. This method constrains the chemical potential (μ), volume (V), and temperature (T) of the MOF–H_2 system to be constant while allowing other thermodynamic quantities to fluctuate.[15] The simulation involves the random insertion/deletion and movement of sorbate molecules within the simulation box until equilibrium is reached. An infinitely extended crystal environment was approximated by periodic boundary conditions with a spherical cut-off of 11.71825 Å, which corresponds to half the unit cell dimension length. All MOF atoms were constrained to be rigid for the simulations, including the atoms of the dimethylammonium counterions. The average particle number was calculated numerically by a statistical mechanical expression based on the grand canonical ensemble.[16,17] The chemical potential for H_2 was determined using the BACK equation of state.[18] Quantum corrections were included in the simulations by using the Feynman-Hibbs potential to the fourth order.[19] All simulations were performed using the Massively Parallel Monte Carlo (MPMC) code, an open-source code that is currently available for download on Google Code.[14]

Many-Body Polarization

An overview of the Thole-Applequist type polarization model[20–22] used in this work is given here. The induced dipole, μ, at site i can be calculated using the following equation:

$$\vec{\mu}_i = \alpha_i^\circ \left(\vec{E}_i^{stat} - \sum_{j \neq i}^{N} \mathbf{T}_{ij} \vec{\mu}_j \right) \tag{2}$$

where α_i° represents the (scalar) atomic point polarizability, $\vec{E}_i^{stat}$ is the static electric field experienced at site i due to the presence of the MOF atoms and the H_2 molecules, $\vec{\mu}_j$ represents the induced dipole at site j, and $\mathbf{T}_{ij}^{\alpha\beta}$ is the dipole field tensor which is defined from electrostatic first-principles as the following:[20]

$$\mathbf{T}_{ij}^{\alpha\beta} = \nabla^\alpha \nabla^\beta \frac{1}{r_{ij}} \tag{3}$$

$$= \frac{\delta^{\alpha\beta}}{r_{ij}^3} - \frac{3x^\alpha x^\beta}{r_{ij}^5} \tag{4}$$

where r_{ij} is the distance between sites i and j. Equation 2 is a self-consistent equation with respect to the dipoles and thus, the quantity $\vec{\mu}_i$ must be solved for using iterative methods for large systems. Note, equation 2 can be solved exactly using matrix inversion, but this is computationally efficient for only small systems. The iterative method employed herein was the Gauss–Seidel relaxation technique.[23] This method consists of updating the current dipole vector set for the k^{th} iteration step as the new dipole vectors become available *via* the following:[24]

$$\vec{\mu}_i^k = \alpha_i^\circ \left(\vec{E}_i^{stat} - \sum_{j \neq i} \hat{T}_{ij} \vec{\mu}_j^{k-1+\zeta} \right) \tag{5}$$

$$\zeta = \begin{cases} 0, & \text{if } i < j \\ 1, & \text{if } i > j \end{cases} \tag{6}$$

In this equation, $\hat{T}_{ij}$ is the modified dipole field tensor that accounts for short range divergences in the polarization model, defined as:[24–26]

$$\hat{T}_{ij}^{\alpha\beta} = \frac{\delta_{\alpha\beta}}{r_{ij}^3} \left[1 - \left(\frac{\lambda^2 r_{ij}^2}{2} + \lambda r_{ij} + 1 \right) e^{-\lambda r_{ij}} \right] - \frac{3x^\alpha x^\beta}{r_{ij}^5} \left[1 - \left(\frac{\lambda^3 r_{ij}^3}{6} + \frac{\lambda^2 r_{ij}^2}{2} + \lambda r_{ij} + 1 \right) e^{-\lambda r_{ij}} \right] \tag{7}$$

where λ is a parameter damping the dipole interactions near the regions of discontinuity. A value of 2.1304 was used for λ in this work, which is consistent with the work performed by B. Thole.[21] The many-body polarization energy for the MOF–H_2 system was calculated by the following based on the work of Palmo and Krimm:[27]

$$U_{pol}^k = -\frac{1}{2} \sum_i \vec{\mu}_i^k \cdot \vec{E}_i^{stat} - \frac{1}{2} \sum_i \vec{\mu}_i^k \cdot \vec{E}_i^{k+1} \tag{8}$$

Thus, the polarization energy was determined from the k^{th} iteration dipoles and the $(k+1)^{th}$ induced field.

Inelastic Neutron Scattering Details

Y-FTZB was synthesized and activated according to the procedure reported by Xue *et al.*[1] The inelastic neutron scattering (INS) spectra for Y-FTZB were collected on the cold neutron time-of-flight spectrometer TOFTOF (at the FRM-II, Munich, Germany) using 0.682 g of the compound. The activated sample was transferred under He into the Al sample holder used for the experiment. The sample holder was attached to the sample stick of the cryostat, connected to a capillary leading to an external gas handling system, and evacuated. Sorption of predetermined amounts of H_2 was carried out *in situ* at 77 K from the external gas handling system, and the INS spectra were collected at a temperature of 1.5 K. The incident energies chosen in these measurements were 25 meV and 9.1 meV, to (respectively) cover a wide range of energy transfers in energy loss, and to resolve the most interesting features in the low energy transfer region. The resulting high resolution (λ = 3.0 Å) and low resolution spectrum (λ = 1.8 Å) at a loading of 2 H_2/Y are provided in Figures S9(a) and S9(b), respectively. The high resolution spectra for different loadings of H_2 are shown in Figure S10.

As explained in the main text, the peak 2.4 meV in the INS spectrum for Y-FTZB corresponds to sorption onto a Y^{3+} ion that is surrounded by four tetrazolate groups and in proximity to a $(CH_3)_2NH_2^+$ counterion. While the most interesting feature in the INS spectrum for Y-FTZB is the peak that appears at 2.4 meV, the sorption sites that give rise to the peaks at approximately 4.0 and 9.0 meV, respectively, have been identified through our simulations. The 4.0 meV peak observed in the INS spectrum corresponds to sorption onto the other chemically distinct Y^{3+} ions in the structure. Although the energetics about these sorption sites are not as strong as the most favorable binding site in the MOF due to the lack of all four surrounding tetrazolate groups and proximal $(CH_3)_2NH_2^+$ counterion, the rotational transition for this site is still lower than the lowest energy peak for most existing MOFs (see next section, Table S7). In addition, according to the phenomenological model,[28] a rotational barrier of 57.6 meV can be associated with the 4.0 meV peak. Even this barrier height is higher than those for MOFs with open-metal Cu^{2+} ions and MOFs that are part of the M-MOF-74 series (Table S7). The peak at approximately 9.0 meV in the INS spectrum as observed in Figure S9(b) corresponds to the sorption of H_2 in the corners of the tetrahedral cage and in proximity to the $(CH_3)_2NH_2^+$ counterions. Although it was observed that H_2 molecules sorbed about uncoordinated counterions have low rotational transitions[29,30] the $(CH_3)_2NH_2^+$ ion is notably bulky and the lower charge/size ratio of this ion results in lower rotational barriers for the sorbed hydrogen. Calculation of the rotational energy levels for a H_2 molecule sorbed in proximity to a counterion revealed a transition in the range of 9.0 to 10.0 meV. This rotational tunneling transition is comparable to those for MOFs that have open-metal Cu^{2+} ions.[31,32]

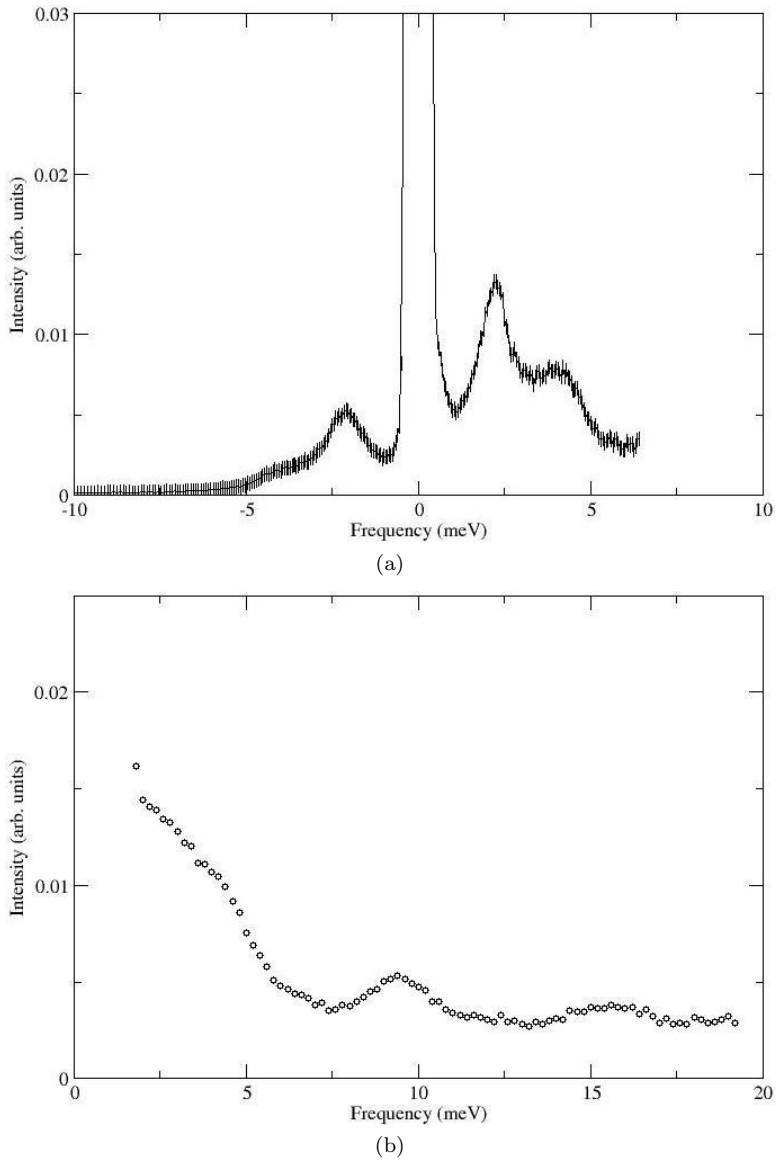

Figure S9. Inelastic neutron scattering (INS) spectra for hydrogen in Y-FTZB at a loading of 2 H_2/Y. **(a)** High resolution spectrum collected with an incident wavelength of 3.0 Å. **(b)** Low resolution spectrum collected with an incident wavelength of 1.8 Å.

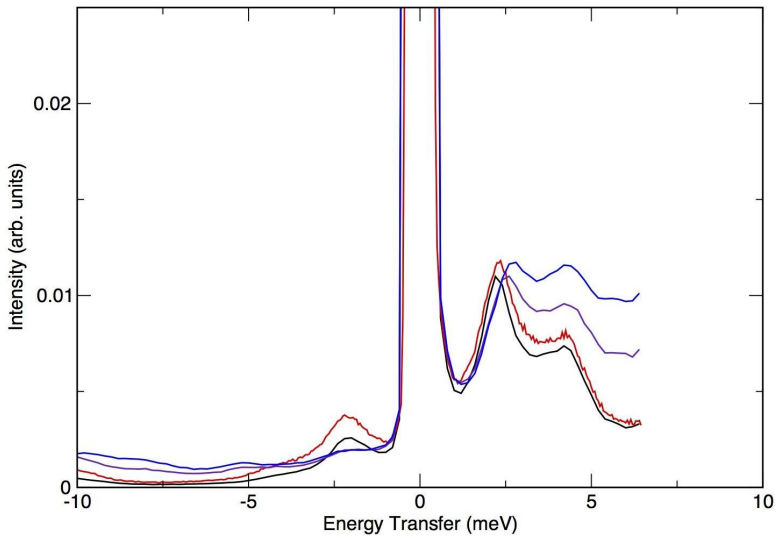

Figure S10. The high resolution inelastic neutron scattering (INS) spectra for hydrogen in Y-FTZB at different loadings: 1 mmol H_2 (black), 2 mmol H_2 (red), 4.2 mmol H_2 (violet), and 6 mmol H_2 (blue). The spectra were collected with an incident wavelength of 3.0 Å.

Comparison of Rotational Barriers

Table S7. A comparison of the lowest energy peaks (0 to 1 transition for the strongest sorption site) observed in the INS spectra for H_2 in various porous materials and their corresponding rotational barriers as calculated using the model in reference 28. The values in parentheses were calculated using a theoretical potential energy surface.

Porous Material	Lowest Energy Peak (meV)	Rotational Barrier (meV)	Reference
LiA	0.85	121.1	33
LiX	1.8	90.1	33
NaX	2.3	79.7	33
Y-FTZB	2.4	78.3 (85.77)	This work
Li-*rho*-ZMOF	3.0	69.5	29
NaA	3.6	62.0	33
DMA-*rho*-ZMOF	4.3	54.4	29
In-*soc*-MOF	4.8	50.0	34
rht-MOF-1	5.0	48.7	30
SIFSIX-2-Cu-i	5.6	47.7 (45.86)	35
Ni-MOF-74	6.6	37.7	36
Mg-MOF-74	6.7/6.8	37.0/36.0	36/37
rht-MOF-7	6.8	36.0	38
Mg-*rho*-ZMOF	7.2	35.3	29
Co-MOF-74	7.7	31.0	36
PCN-12	7.7	31.0	32
Zn-MOF-74	8.3	28.0 (27)	39 (40)
PCN-6	8.7	25.8	41
PCN-6′	8.85	25.0	41
IRMOF-11	8.9	24.8	42
rht-MOF-4a	9.0	24.0	43
HKUST-1	9.1	23.7	31
MOF-177	9.7	20.4	42
SIFSIX-2-Cu	10.5	17.0	35
IRMOF-8	10.8	15.6	42

Quantum Rotation Calculations

The two-dimensional quantum rotational levels for a H_2 molecule sorbed at a sorption site in Y-FTZB were calculated by diagonalizing the rotor Hamiltonian in the spherical harmonic basis, Y_{jm}, which is the following:

$$\hat{H} = B\mathbf{j}^2 + V(\theta, \phi) \tag{9}$$

where B is the rotational constant for molecular hydrogen, which is equal to approximately 85.35 K,[44] $\mathbf{j}^2$ is the angular momentum operator, and $V(\theta,\phi)$ is the potential energy surface for the rotation of the H_2 molecule with its center-of-mass held fixed within the MOF–H_2 system. Each matrix element, $\langle Y_{jm}|V(\theta,\phi)|Y_{jm}\rangle$, was constructed using Gauss-Legendre quadrature[45] with a basis set consisting of $\pm m$ functions.[24] The matrix was diagonalized using the LAPACK linear algebra package,[46] yielding the rotational energy eigenvalues and the eigenvector coefficients. The two-dimensional rotational levels were calculated with $j = 7$, leading to 64 basis functions. The calculated rotational levels for a H_2 molecule sorbed about the most favorable sorption site in Y-FTZB are provided in Table S8.

The rotational barrier was determined by calculating the potential energy of the MOM–H_2 system as the H_2 molecule is rotated at various angles of θ (0 to 180°) and ϕ (0 to 360°). Single point energies were obtained on a sphere (4,096 points based on 64 × 64 Gaussian quadrature integration) and the rotational barrier was calculated by taking the difference between the high and low values. All calculations were performed using the Massively Parallel Monte Carlo (MPMC) code, which is currently available for download on Google Code.[14]

Table S8. The calculated two-dimensional quantum rotational levels for a H_2 molecule sorbed about the most favorable sorption site in Y-FTZB as shown in Figure 3 in the main text. Relative energies are given in meV.

n	j	Calc. ΔE (meV)
1	0	0.00
2		2.74
3	1	24.65
4		40.44
5		44.59
6		46.45
7	2	54.60
8		72.85
9		83.45

[1] Xue, D.-X.; Cairns, A. J.; Belmabkhout, Y.; Wojtas, L.; Liu, Y.; Alkordi, M. H.; Eddaoudi, M. *Journal of the American Chemical Society* **2013**, *135*, 7660–7667.
[2] Jones, J. *Proceedings of the Royal Society of London. Series A, Containing Papers of a Mathematical and Physical Character* **1924**, *106*, 463–477.
[3] Rappé, A. K.; Casewit, C. J.; Colwell, K. S.; Goddard, W. A.; Skiff, W. M. *Journal of the American Chemical Society* **1992**, *114*, 10024–10035.
[4] van Duijnen, P. T.; Swart, M. *The Journal of Physical Chemistry A* **1998**, *102*, 2399–2407.
[5] Neese, F. *Wiley Interdisciplinary Reviews: Computational Molecular Science* **2012**, *2*, 73–78.
[6] Chirlian, L. E.; Francl, M. M. *Journal of Computational Chemistry* **1987**, *8*, 894–905.
[7] Breneman, C. M.; Wiberg, K. B. *Journal of Computational Chemistry* **1990**, *11*, 361–373.
[8] Valiev, M.; Bylaska, E.; Govind, N.; Kowalski, K.; Straatsma, T.; Dam, H. V.; Wang, D.; Nieplocha, J.; Apra, E.; Windus, T.; de Jong, W. *Computer Physics Communications* **2010**, *181*, 1477–1489.
[9] Cornell, W. D.; Cieplak, P.; Bayly, C. I.; Gould, I. R.; Merz, K. M.; Ferguson, D. M.; Spellmeyer, D. C.; Fox, T.; Caldwell, J. W.; Kollman, P. A. *Journal of the American Chemical Society* **1995**, *117*, 5179–5197.
[10] Stevens, W. J.; Basch, H.; Krauss, M. *Journal of Chemical Physics* **1984**, *81*, 6026–6033.
[11] Hay, P. J.; Wadt, W. R. *Journal of Chemical Physics* **1985**, *82*, 270–283.
[12] LaJohn, L. A.; Christiansen, P. A.; Ross, R. B.; Atashroo, T.; Ermler, W. C. *Journal of Chemical Physics* **1987**, *87*, 2812–2824.
[13] Belof, J. L.; Stern, A. C.; Space, B. *Journal of Chemical Theory and Computation* **2008**, *4*, 1332–1337.
[14] Belof, J. L.; Space, B. Massively Parallel Monte Carlo (MPMC). Available on Google Code, 2012.
[15] Metropolis, N.; Rosenbluth, A. W.; Rosenbluth, M. N.; Teller, A. H.; Teller, E. *Physics Letters B* **1953**, *21*, 1087–1092.
[16] McQuarrie, D. A. *Statistical Mechanics*; University Science Books: Sausalito, CA, 2000; pp. 53.
[17] Frenkel, D.; Smit, B. *Understanding Molecular Simulation: From Algorithms to Applications*; Academic Press: New York, 2002; pp. 129.
[18] Boublík, T. *Fluid Phase Equilibria* **2005**, *240*, 96–100.
[19] Feynman, R. P.; Hibbs, A. R. *Quantum Mechanics and Path Integrals*; McGraw-Hill: New York, 1965; pp. 281.
[20] Applequist, J.; Carl, J. R.; Fung, K.-K. *Journal of the American Chemical Society* **1972**, *94*, 2952–2960.
[21] Thole, B. *Chemical Physics* **1981**, *59*, 341 – 350.
[22] Bode, K. A.; Applequist, J. *The Journal of Physical Chemistry* **1996**, *100*, 17820–17824.
[23] Dinh, T.-L.; Huber, G. A. *Journal of Mathematical Modelling and Algorithms* **2005**, *4*, 111–128.
[24] Belof, J. L. Theory and simulation of metal-organic materials and biomolecules. Ph.D. thesis, University of South Florida, 2009.
[25] Belof, J. L.; Stern, A. C.; Eddaoudi, M.; Space, B. *Journal of the American Chemical Society* **2007**, *129*, 15202–15210, PMID: 17999501.
[26] Forrest, K. A.; Pham, T.; McLaughlin, K.; Belof, J. L.; Stern, A. C.; Zaworotko, M. J.; Space, B. *The Journal of Physical Chemistry C* **2012**, *116*, 15538–15549.
[27] Palmo, K.; Krimm, S. *Chemical Physics Letters* **2004**, *395*, 133–137.
[28] Nicol, J. M.; Eckert, J.; Howard, J. *The Journal of Physical Chemistry* **1988**, *92*, 7117–7121.
[29] Nouar, F.; Eckert, J.; Eubank, J. F.; Forster, P.; Eddaoudi, M. *Journal of the American Chemical Society* **2009**, *131*, 2864–2870, PMID: 19206515.
[30] Pham, T.; Forrest, K. A.; Hogan, A.; McLaughlin, K.; Belof, J. L.; Eckert, J.; Space, B. *Journal of Materials Chemistry A* **2014**, *2*, 2088–2100.
[31] Brown, C. M.; Liu, Y.; Yildirim, T.; Peterson, V. K.; Kepert, C. J. *Nanotechnology* **2009**, *20*, 204025.
[32] Wang, X.-S.; Ma, S.; Forster, P.; Yuan, D.; Eckert, J.; López, J.; Murphy, B.; Parise, J.; Zhou, H.-C. *Angewandte Chemie International Edition* **2008**, *47*, 7263–7266.
[33] Eckert, J.; Trouw, F. R.; Mojet, B.; Forster, P.; Lobo, R. *Journal of Nanoscience and Nanotechnology* **2010**, *10*, 49–59.
[34] Liu, Y.; Eubank, J. F.; Cairns, A. J.; Eckert, J.; Kravtsov, V. C.; Luebke, R.; Eddaoudi, M. *Angewandte Chemie International Edition* **2007**, *46*, 3278–3283.
[35] Nugent, P.; Pham, T.; McLaughlin, K.; Georgiev, P. A.; Lohstroh, W.; Embs, J. P.; Zaworotko, M. J.; Space, B.; Eckert, J. *Journal of Materials Chemistry A* **2014**, DOI: 10.1039/c4ta02171a.
[36] Dietzel, P. D. C.; Georgiev, P. A.; Eckert, J.; Blom, R.; Strassle, T.; Unruh, T. *Chemical Communications* **2010**, *46*, 4962–4964.
[37] Sumida, K.; Brown, C. M.; Herm, Z. R.; Chavan, S.; Bordiga, S.; Long, J. R. *Chemical Communications* **2011**, *47*, 1157–1159.
[38] Pham, T.; Forrest, K. A.; Eckert, J.; Georgiev, P. A.; Mullen, A.; Luebke, R.; Cairns, A. J.; Belmabkhout, Y.; Eubank, J. F.; McLaughlin, K.; Lohstroh, W.; Eddaoudi, M.; Space, B. *The Journal of Physical Chemistry C* **2014**, *118*, 439–456.
[39] Liu, Y.; Kabbour, H.; Brown, C. M.; Neumann, D. A.; Ahn, C. C. *Langmuir* **2008**, *24*, 4772–4777.
[40] Kong, L.; Román-Pérez, G.; Soler, J. M.; Langreth, D. C. *Physical Review Letters* **2009**, *103*, 096103.
[41] Ma, S.; Eckert, J.; Forster, P. M.; Yoon, J. W.; Hwang, Y. K.; Chang, J.-S.; Collier, C. D.; Parise, J. B.; Zhou, H.-C. *Journal of the American Chemical Society* **2008**, *130*, 15896–15902.
[42] Rowsell, J. L. C.; Eckert, J.; Yaghi, O. M. *Journal of the American Chemical Society* **2005**, *127*, 14904–14910, PMID: 16231946.
[43] Eubank, J. F.; Nouar, F.; Luebke, R.; Cairns, A. J.; Wojtas, L.; Alkordi, M.; Bousquet, T.; Hight, M. R.; Eckert, J.; Embs, J. P.; Georgiev, P. A.; Eddaoudi, M. *Angewandte Chemie International Edition* **2012**, *51*, 10099–10103.
[44] Bigeleisen, J.; Mayer, M. G. *Journal of Chemical Physics* **1947**, *15*, 261.
[45] Abramowitz, M. *Handbook of Mathematical Functions with Formulas, Graphs, and Mathematical Tables* **1965**, Chapt. 25, Sect. 4, pg. 887.
[46] Anderson, E.; Bai, Z.; Dongarra, J.; Greenbaum, A.; McKenney, A.; Du Croz, J.; Hammerling, S.; Demmel, J.; Bischof, C.; Sorensen, D. LAPACK: A portable linear algebra library for high-performance computers. Proceedings of the 1990 ACM/IEEE conference on Supercomputing. 1990; pp 2–11.